Gas-Phase Reactions between Urea and Ca^{2+}: The Importance of Coulomb Explosions

Inés Corral,[†] Otilia Mó,[†] Manuel Yáñez,*[,†] Jean-Yves Salpin,[‡] Jeanine Tortajada,*[,‡] and Leo Radom*[,§]

Departamento de Química, C-9, Universidad Autónoma de Madrid, Cantoblanco, 28049-Madrid, Spain, Laboratoire Analyse et Environnement, UMR CNRS 8587, Université d'Evry Val d'Essonne, Institut des Sciences, Boulevard François Mitterrand, 91025 EVRY CEDEX, France, School of Chemistry, University of Sydney, Sydney, NSW 2006, Australia, and Research School of Chemistry, Australian National University, Canberra, ACT 0200, Australia

Received: July 28, 2004

The gas-phase reactions between urea and Ca^{2+} have been investigated by means of electrospray mass spectrometry techniques. The MS/MS spectra of $[Ca(urea)]^{2+}$ and $[Ca(urea-H)]^{+}$ complexes show that both ions decompose by losing NH_3 and HNCO. However, for the $[Ca(urea)]^{2+}$ system, additional intense peaks are observed at *m*/*z* 44, 56, and 82. Density functional theory calculations at the B3-LYP/cc-pWCVTZ level have been used to help rationalize these observations through an examination of the structures and bonding characteristics of the various stationary points on the $[Ca(urea)]^{2+}$ and $[Ca(urea-H)]^{+}$ potential energy surfaces (PESs). Analysis of the topology of these PESs allows mechanisms to be proposed for the loss of NH_3 and HNCO. In addition, for $[Ca(urea)]^{2+}$, the calculations suggest that the *m*/*z* 44, 56, and 82 peaks correspond to H_2NCO^+, $CaNH_2^+$, and $[Ca, N, C, O]^+$, respectively, which are produced in Coulomb explosion processes. The unimolecular reactivity of $[Ca(urea-H)]^{+}$ differs from that of $[Ca(urea)]^{2+}$ largely through the absence of the Coulomb explosion fragmentations. Urea behaves as an oxygen base with respect to Ca^{2+}, the calculated binding energy being 453 kJ mol^{-1}.

Introduction

Divalent cations play an important role in biological systems.[1−4] It is well established, for example, that the association of transition-metal dications with DNA bases facilitates their thermal denaturation[5] and increases the melting temperature of the DNA double helix.[6] Also, divalent transition-metal cations stabilize some DNA triplexes[7] and increase the base-pair dissociation energy.[8] Divalent alkaline earth metal dications (Mg^{2+}, Ca^{2+}, Ba^{2+}) seem to interact exclusively in these cases with the phosphate group,[9,10] but they are also involved in many other biological processes. For example, some specific proton-transfer mechanisms between guanine and cytosine in Watson−Crick base pairs are triggered by doubly charged alkaline earth metal cations.[10] The alkaline earth dications also stabilize rybozimes.[11]

It is clear that in order to understand the role of metal cations in the biochemistry of DNA it is important to have detailed knowledge of the interaction of these ions with the individual bases. This has motivated a great deal of interest in the theoretical study of the interaction of metal mono- and dications with different DNA components such as guanine or adenine,[12,13] with Watson−Crick base pairs[14] such as guanine-cytosine[8] or adenine-thymine,[15] and with reverse-Hoogsteen base pairs[15] such as adenine-adenine. Extensions of these studies to interactions involving hydrated metal dications have also been reported in the literature.[16−19]

Most of the theoretical investigations published to date on such systems have concentrated on the structures and relative stabilities of the possible ion−molecule complexes and on providing reasonable metal cation binding energies.[20−22] Very little is known about the reactivity of the systems upon cation attachment. From an experimental point of view, the development of electrospray ionization techniques has opened up the possibility of producing clusters involving metal dications in the gas phase from aqueous solution[23] and therefore of gaining direct information about the intrinsic reactivity of organic molecules when interacting with metal dications.

One reasonable way of approaching the problem of the reactivity of large biochemical compounds such as the nucleotides is by exploring the behavior of small model systems such as guanidine, formamide, and urea, which include the key functional groups. This is the approach that we have previously followed[24−27] to investigate the reactivity of nucleotides with respect to different metal monocations, and this is the approach that we will use to study their reactivity with regard to metal dications. Initially, we have focused our attention on processes involving Ca^{2+} because of its biological relevance.

To obtain a more detailed picture of the reactivity patterns, one needs not only to have experimental information about the product distributions but also to postulate appropriate reaction mechanisms based on the topology of the potential energy surface. A reliable description of this topology requires theoretical procedures that are sufficiently accurate to be able to predict the relative stabilities of the various local minima, transition structures, and dissociation products reliably. For this reason, in a previous paper[28] we carried out an assessment of theoretical procedures for the description of the interactions between neutral molecules and Ca^{2+}. In that study, we concluded that the B3-LYP density functional method in conjunction with a cc-pWCVTZ basis set provides a good compromise between accuracy and computational cost in the calculation of the

* Corresponding authors. E-mail: manuel.yanez@uam.es; jeanine.tortajada@chemie.univ-evry.fr; radom@chem.usyd.edu.au.
[†] Universidad Autónoma de Madrid.
[‡] Université d'Evry Val d'Essonne.
[§] University of Sydney and Australian National University.

10.1021/jp046624z CCC: $27.50
Published on Web 10/14/2004

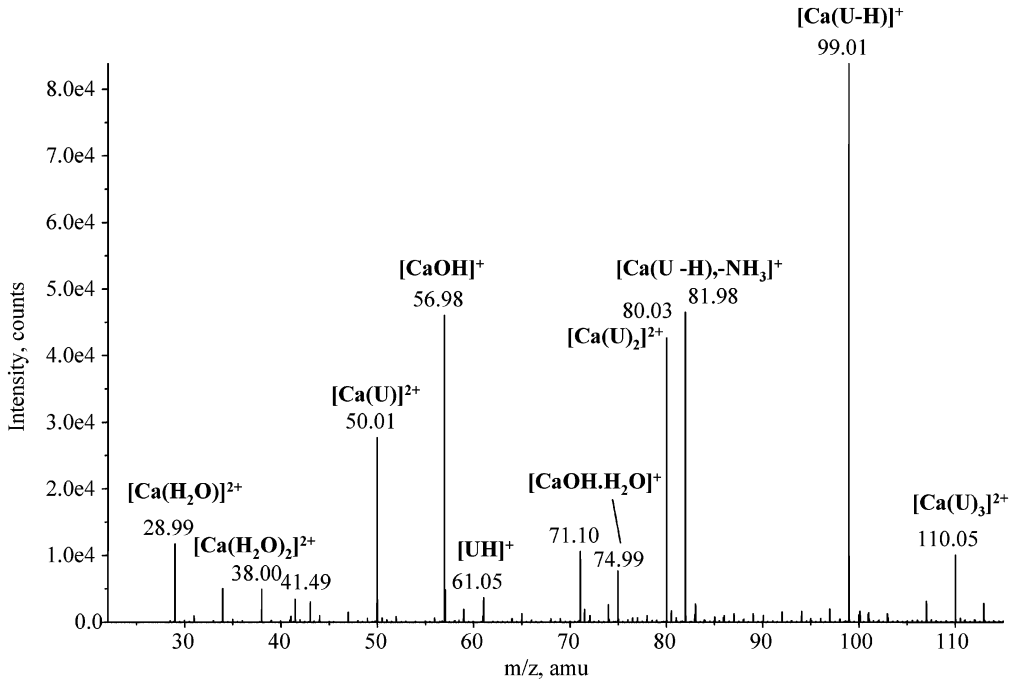

Figure 1. Positive-ion electrospray mass spectrum of an aqueous $CaCl_2$/urea (10^{-4} mol L^{-1}/10^{-4} mol L^{-1}) solution.

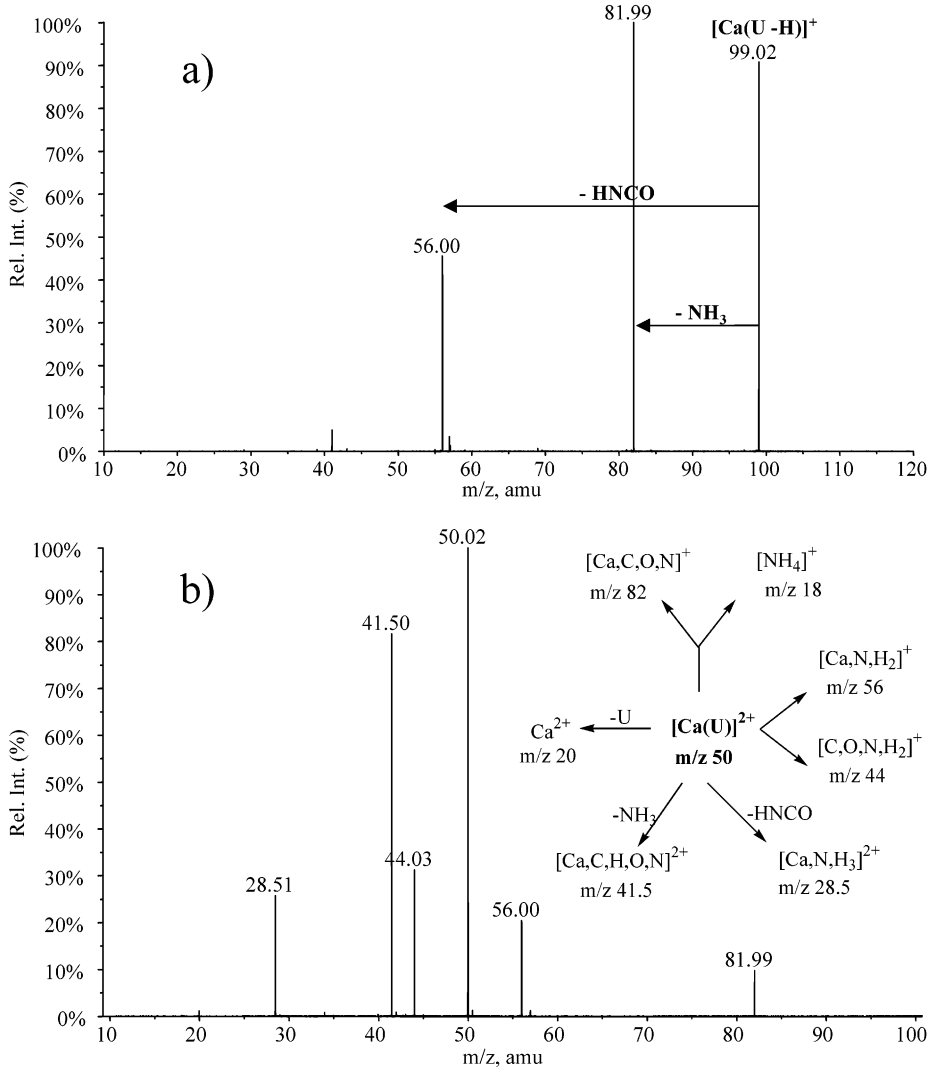

Figure 2. Low-energy CID spectra of (a) $[Ca(U-H)]^+$ and (b) $[Ca(U)]^{2+}$ complexes recorded at DP = 30 V and E_{lab} = 11 and 13 eV, respectively. Intensities are given relative to that of the base peak.

structures and binding energies for Ca^{2+} complexes. Hence, this will be the theoretical procedure used in the present work.

Experimental Section

Electrospray mass spectra were recorded on a QSTAR PULSAR i (Applied Biosystems/MDS Sciex) hybrid instrument (QqTOF) fitted with an "ion spray" source. Aqueous mixtures of calcium chloride and urea (10^{-4} mol L^{-1}/10^{-4} mol L^{-1}) were introduced into the source using direct infusion with a syringe pump at a flow rate of 4 μL/min. Ionization of the samples was achieved by applying a voltage of 5.4 kV to the sprayer probe and by the use of a nebulizing gas (GAS1, air) surrounding the sprayer probe. The operating pressure of GAS1 was adjusted to 1.4 bar by means of an electronic board (pressure sensors) as a fraction of the air inlet pressure. The curtain gas (N_2), which prevents air or solvent from entering the analyzer region, was similarly adjusted to a value of 1.4 bar. During the experiments, the collision gas (CAD, N_2) was on at all times for collisional focusing in both Q0 (ion guide preceding Q1) and Q2 (collision cell) to improve ion transmission and subsequently sensitivity.

For MS/MS spectra, ions of interest were mass selected using Q1 and allowed to collide at variable collision energies with nitrogen as collision gas in the second quadrupole (Q2), the resulting fragments being separated by the TOF analyzer after orthogonal injection. Low gas pressures in the cell (typically 10^{-5} mbar) were used so as to limit multiple ion−molecule collisions. The declustering potential (DP), defined as the difference in potential between the orifice plate and the skimmer (grounded) and typically referred to as the "cone voltage" for other electrospray interfaces, ranged from 30 to 50 V. Furthermore, MS/MS spectra were systematically recorded at different collision energies. (The kinetic energy of the ions is given by the difference in potential between the focusing quadrupole Q0 preceding Q1 and the collision cell Q2.)

Urea and calcium chloride were purchased from Aldrich and were used without further purification. All of the measurements presented in this paper were carried out in 100% water purified with a Milli-Q water purification system.

Computational Details

Standard density functional theory calculations[29] were performed on neutral urea (U) and on $[Ca(U)]^{2+}$ and $[Ca(U-H)]^{+}$ complexes using the Gaussian 98 suite of programs.[30] Optimized geometries and harmonic vibrational frequencies were obtained with the B3-LYP[31,32] procedure, combined with cc-pWCVTZ basis sets.[33] The same theoretical scheme was used to obtain structural and energetic information about other stationary points of the $[Ca(U)]^{2+}$ and $[Ca(U-H)]^{+}$ potential energy surfaces (PES). The harmonic vibrational frequencies were also used to classify the stationary points as local minima or saddle points and to estimate the zero-point vibrational energy (ZPVE) corrections, obtained using a scaling factor of 0.985.[34] To determine the connectivity between each transition structure and its adjacent minima, we have used the intrinsic reaction coordinate (IRC) procedure, as implemented in Gaussian 98.[35]

Binding energies were calculated, at the same levels of theory used for geometry optimizations, as the difference between the energy of the most stable $[Ca(U)]^{2+}$ complex and the energy of Ca^{2+} plus the energy of urea in its most stable conformation, after including the ZPVE corrections.

The bonding within the individual equilibrium structures was analyzed by locating the bond critical points (bcps) using atoms-in-molecules (AIM) theory,[36] which is based on a topological analysis of the charge density. On one hand, the calculation of the different bcps and the corresponding bond paths leads to a clear definition of the corresponding molecular graph, and on the other hand, the electron density at the bcps is a good measure of the strength of the bond.

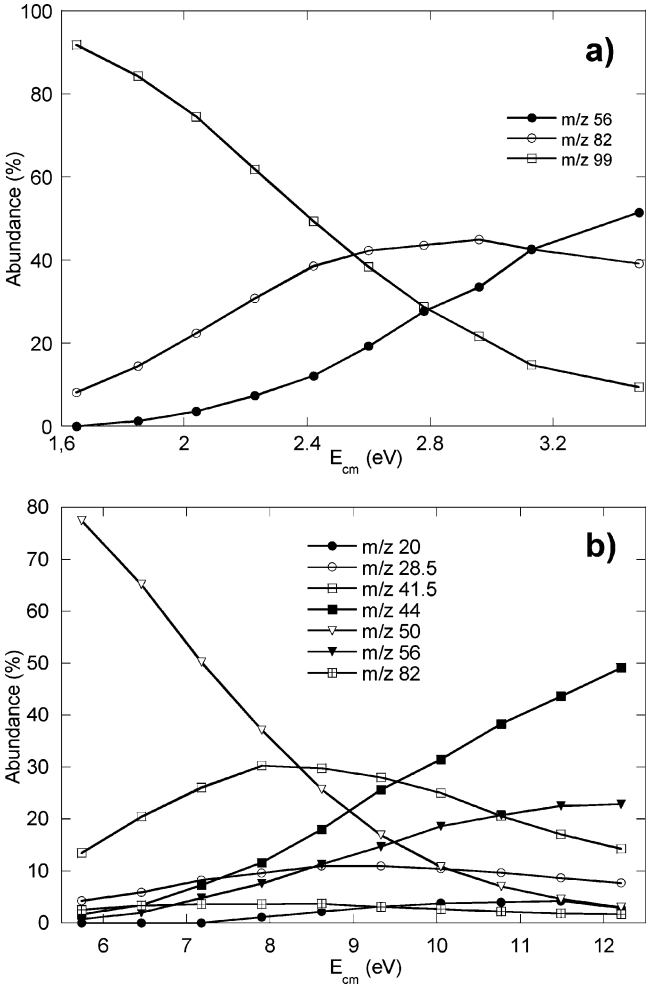

Figure 3. Intensity of fragment ions generated upon CID of (a) $[Ca(U-H)]^{+}$ and (b) $[Ca(U)]^{2+}$ ions as a function of the center-of-mass collision energy (E_{cm}). The abundances correspond to the percentage of the total ion current for each ion.

Results and Discussion

Mass Spectrometry Observations. Figure 1 presents the electrospray mass spectrum obtained at DP = 30 V for a 1:1 aqueous mixture of $CaCl_2$/urea. Several types of ions can be observed. The first group corresponds to hydrated Ca ions $[Ca(H_2O)_n]^{2+}$ (n = 1, 2, and 3) at m/z 29, 38, and 47 (not labeled in Figure 1), respectively. These ions are less intense than calcium hydroxide $CaOH^{+}$ (m/z 57) for all of the DP values used and disappear progressively as the DP increases. Interaction between urea and the calcium ion gives rise to both singly and doubly charged complexes. Ions of general formula $[Ca(U)_n]^{2+}$ (n = 1, 2, and 3) are detected in significant abundance at m/z 50, 80, and 110. However, their observation is not straightforward and requires soft energetic source/interface conditions (low DP). Their intensity reaches a maximum when the DP is set to 0 V. Increasing the declustering potential results in the fragmentation of the doubly charged ions and in the appearance of a deprotonated $[Ca(U-H)]^{+}$ complex at m/z 99. This latter ion is in fact found to be the most abundant species formed from Ca^{2+} and urea, regardless of the DP value used.

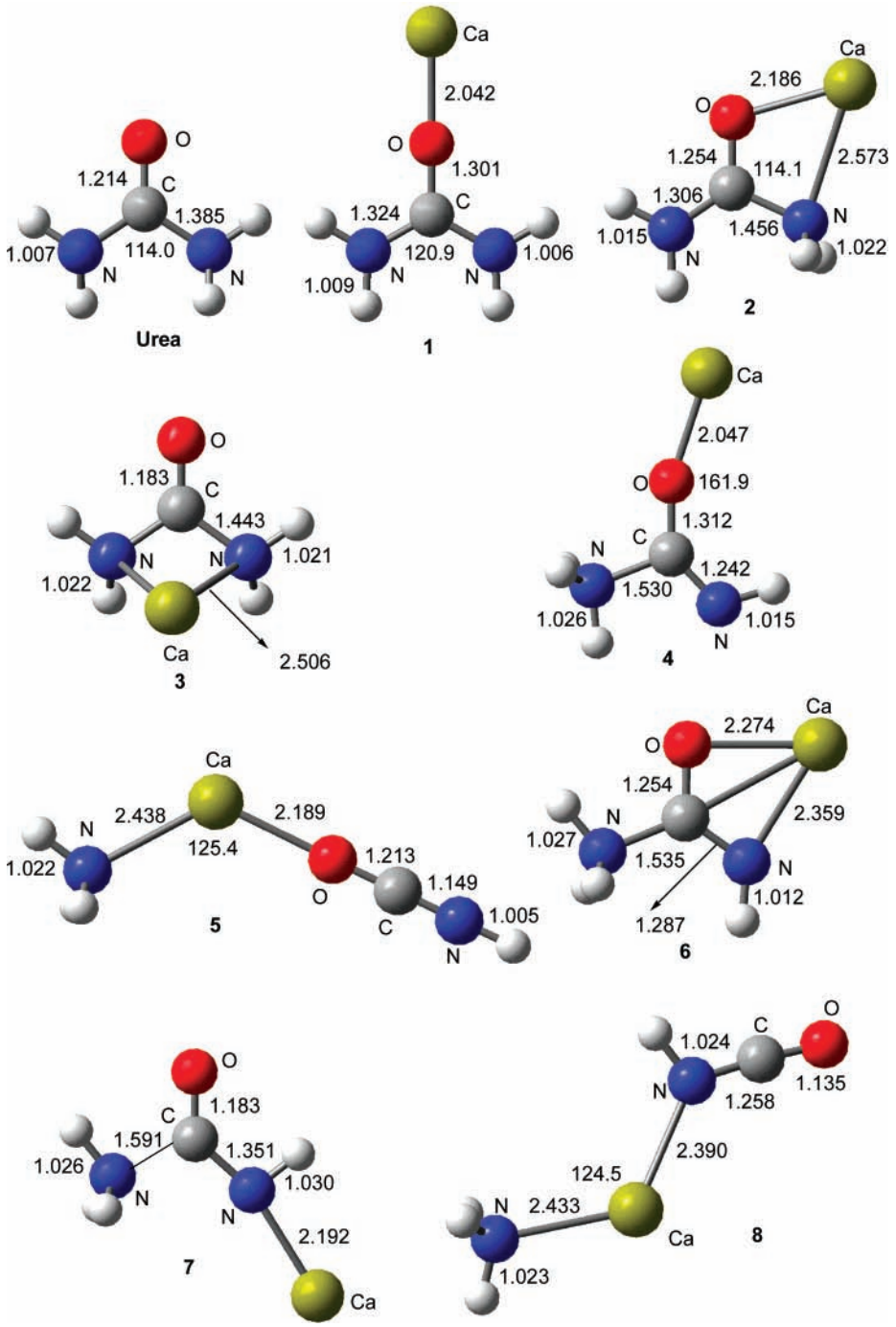

Figure 4. Optimized geometries for urea and isomeric $[Ca(urea)]^{2+}$ structures. Bond lengths are in angstroms, and bond angles are in degrees.

We will now focus on the $[Ca(U-H)]^+$ and the $[Ca(U)]^{2+}$ MS/MS spectra. These spectra have been recorded at DP = 30 V, a value for which sufficient intensities of both singly and doubly charged complexes are obtained. Typical CID spectra for the $[Ca(U)]^{2+}$ and $[Ca(U-H)]^+$ species are given in Figure 2, and Figure 3 illustrates the evolution of product ion intensities as a function of the center-of-mass collision energy. Note that on our instrument and for this particular system the smallest value of the collision energy in the laboratory frame (E_{lab}) for which a sufficient number of fragment ions can reach the detector was 8 eV, and at this value, dissociation of the parent ions has already occurred. This corresponds to center-of-mass collision energies of 1.76 and 5.74 eV for *m*/*z* 99 and 50, respectively. These two complexes exhibit two common fragmentations: loss of ammonia and elimination of a molecule of 43 Da [H, N, C, O]. These two processes have already been encountered in reactions of urea with Cu^+ [26,37] and Ni^+ [38] ions. From an examination of Figure 3, we can see that the loss of [H, N, C, O] from the singly charged complex becomes dominant after E_{cm} = 3.1 eV, whereas the loss of ammonia always remains preponderant for the dication. Unlike the corresponding situations for Cu^+ or Ni^+, the loss of water, which has been attributed to a partial collision-induced isomerization of $[M(\mathbf{U})]^+$ (M = metal) in the cone region prior to mass selection,[37,38] is not observed. Moreover, we do not detect any ion corresponding to the loss of CO. The elimination of urea occurs solely for the doubly charged complex, but only to a very minor extent and at high collision energy.

Additional fragmentations (*m*/*z* 44, 56, 82) that we attribute to two Coulomb explosion processes (i.e., fragmentation of the

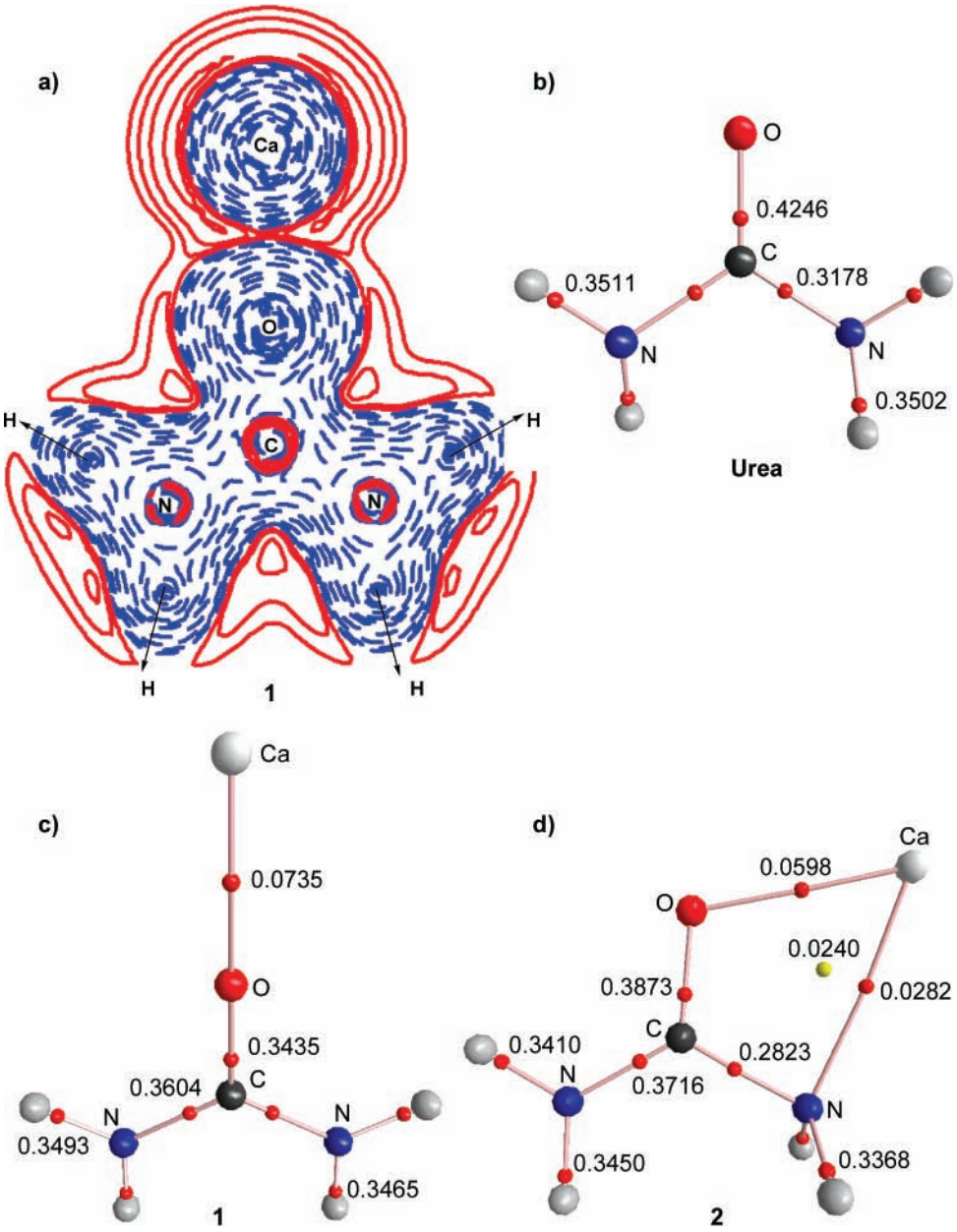

Figure 5. (a) Contour map of the energy density for the most stable $[Ca(urea)]^{2+}$ complex (**1**). Blue dashed lines correspond to negative values of H(**r**), and solid red lines correspond to positive values. (b−d) Molecular graphs of urea and complexes **1** and **2** showing the bcps (red) and the ring critical points (yellow). Electron densities are in au.

$[Ca(U)]^{2+}$ dication into two monocations) are observed for the $[Ca(U)]^{2+}$ complex. These fragmentations are summarized in the scheme included in Figure 2b. The $[Ca, C, H, O, N]^{2+}$ ion (*m*/*z* 41.5) prevails at low collision energies (below 9.5 eV), whereas the charge-separation process, leading to the *m*/*z* 56/44 pair, clearly dominates at high collision energies (Figure 3b). Note that the *m*/*z* 18 ion ($[NH_4]^+$) is observed only at very high collision energy and to a very minor extent.

To rationalize these experimental findings, we have carried out theoretical calculations that enable us to discuss the topology of the $[Ca(U)]^{2+}$ and $[Ca(U-H)]^+$ PESs as well as the structures and bonding characteristics of the most stable complexes.

Structures and Relative Stabilities of $[Ca(U)]^{2+}$ Isomers. The most stable structure of the $[Ca(U)]^{2+}$ complex (**1**) corresponds to the association of the metal dication with the carbonyl oxygen (Figure 4), in agreement with previous findings about the preference of Ca^{2+} to bind to oxygen atoms.[8,10] A second local minimum (**2**), in which Ca^{2+} bridges between the carbonyl oxygen and one of the amino groups, lies 43 kJ mol^{-1} higher in energy. A third local minimum (**3**), with the metal dication bridging between the two amino groups, lies 130 kJ mol^{-1} above **1**. The geometries of the other local minima of the PES that can be obtained from these adducts by appropriate hydrogen shifts are also included in Figure 4. For the remaining stationary points, the geometries are given in Table S1 of the Supporting Information. The total energies as well as the zero-point energies of all of the stationary points on the $[Ca(U)]^{2+}$ potential energy surface are given in Table S2.

A topological analysis of the charge density of these complexes reveals that the Ca^{2+}−urea interaction is essentially electrostatic, as indicated by the positive value of the energy density in the region between the two interacting subunits (Figure 5a). However, the strong polarization effects caused by the metal dication are reflected in nonnegligible bond perturbations. As can be seen from Figure 5b and c, there is a decrease in the electron density at the C═O bond critical point on going

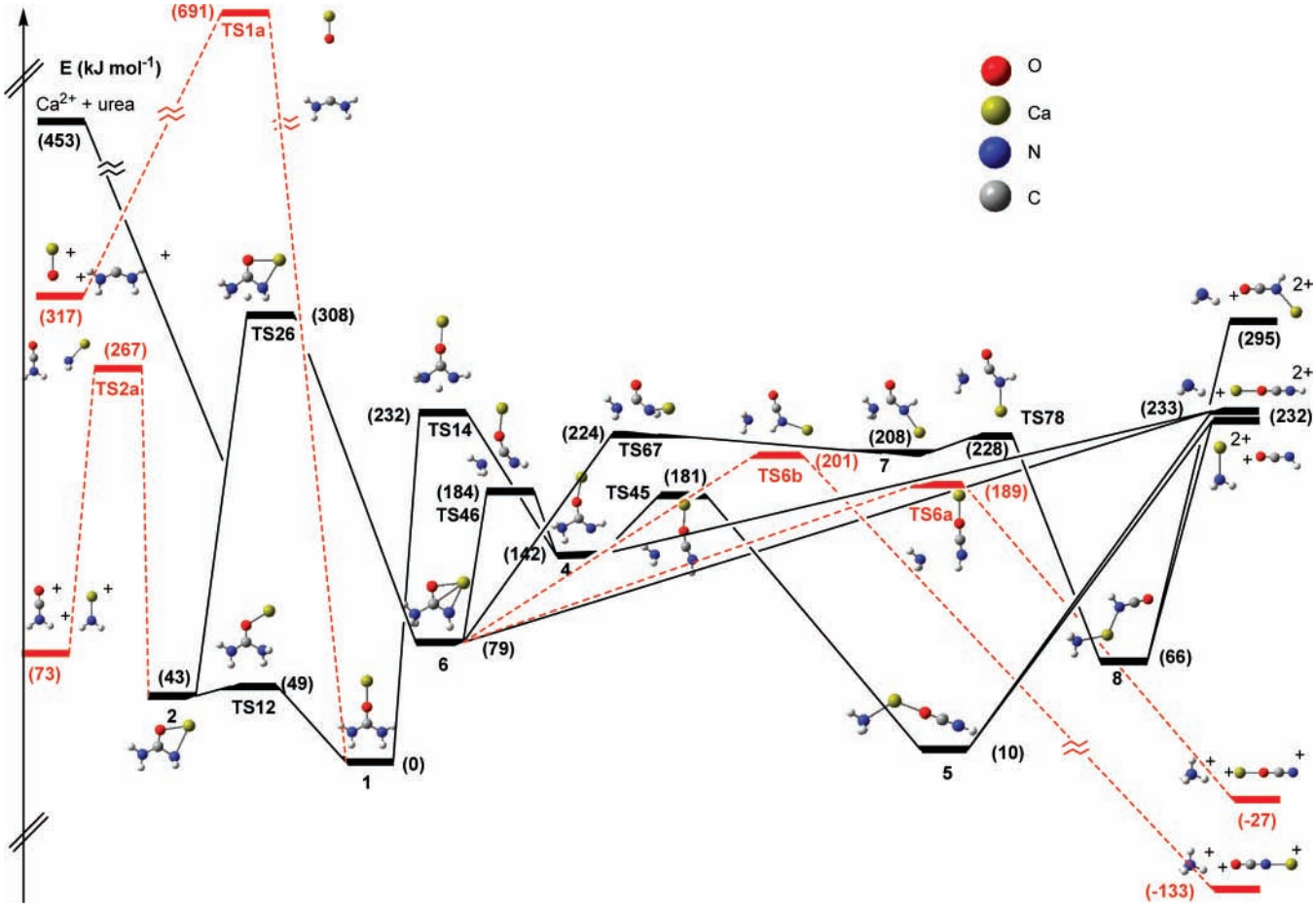

Figure 6. Schematic energy profile for reactions of $[Ca(urea)]^{2+}$. Black solid lines indicate mechanisms associated with the loss of neutral fragments. Dashed red lines correspond to mechanisms associated with Coulomb explosion processes. Relative energies (kJ mol^{-1}) are in parentheses.

from neutral urea to complex **1**. Accordingly, the C═O bond length increases by 0.087 Å, and its stretching frequency is red shifted by 234 cm^{-1}. Concomitantly, the charge density at the C−N bcps increases as a consequence of an increase in the conjugation of the nitrogen lone pairs, triggered by the polarization caused by the metal dication. Interestingly, the urea moiety in complex **1** is strictly planar, whereas in the free molecule, both amino groups are slightly pyramidalized. The C−N bond strengthening is mirrored in a shortening of the C−N bonds by 0.061 Å and in the blue shifting (by 114 and 291 cm^{-1}, respectively) of the corresponding symmetric and antisymmetric C−N stretching frequencies.

Sizable bonding changes are also evident in complex **2**. The most significant one is the weakening of the C−N bond involving the amino group bonded to the metal cation and the strengthening of the C−N bond involving the free amino group. The bond length of the former increases by 0.071 Å, its stretching frequency appears to be red shifted by 220 cm^{-1}, and the charge density at the bcp decreases by 0.036 au, whereas the bond length of the latter decreases by 0.079 Å, its stretching frequency appears to be blue shifted by 332 cm^{-1}, and the charge density at the bcp increases by 0.054 au.

These polarization effects are also mirrored in the large binding energy between Ca^{2+} and urea in **1** (453 kJ mol^{-1}), which is substantially larger than the calculated value for the interaction of Ca^{2+} with water (230 kJ mol^{-1})[22] and also much larger than that calculated at the same level of theory for the interaction of Ca^{2+} with formaldehyde (272.7 kJ mol^{-1}),[28] reflecting the substantial effect of the two amino groups on the intrinsic basicity of the carbonyl group.

Mechanisms for the Unimolecular Reactions of $[Ca(U)]^{2+}$ Ions. A schematic potential energy profile corresponding to the unimolecular reactions of the $[Ca(U)]^{2+}$ complex is displayed in Figure 6. We have distinguished those mechanisms associated with the loss of a neutral fragment (black solid lines) from those that correspond to the formation of two monocations through Coulomb explosion processes (red dashed lines).

Starting from the global minimum, **1**, two straightforward isomerization reactions can be envisaged. These are the migration of Ca^{2+} accompanied by the rotation of one of the amino groups via **TS12**, leading to the secondary local minimum, **2**, and the 1,3-H shift from one amino group to the other, via the transition structure **TS14**, to yield structure **4**. Structure **4** may directly lose NH_3, which corresponds to the main peak in the MS/MS spectrum. Alternatively, the ammonia molecule attached to the carbon atom in **4** can migrate, via the transition structure **TS45**, to yield a very stable complex, **5,** in which ammonia is now attached to Ca. This complex can dissociate by losing either NH_3 or HNCO, the two processes having virtually the same energy requirements.

Mechanisms for the loss of NH_3 and HNCO that have their origin in local minimum **2** appear unlikely to play a significant role because the 1,3-H shift between the two amino groups that leads, via **TS26**, to the relevant intermediate **6** has a large barrier. However, there is an alternative route to **6**, starting from **1** via **4**. This isomerization process takes place through an inversion of the imino group via a transition structure that lies 184 kJ mol^{-1} above the global minimum. Complex **6** can directly lose NH_3 in a manner similar to that postulated above for complex **4**. Alternatively, complex **6** can isomerize, in a two-step process

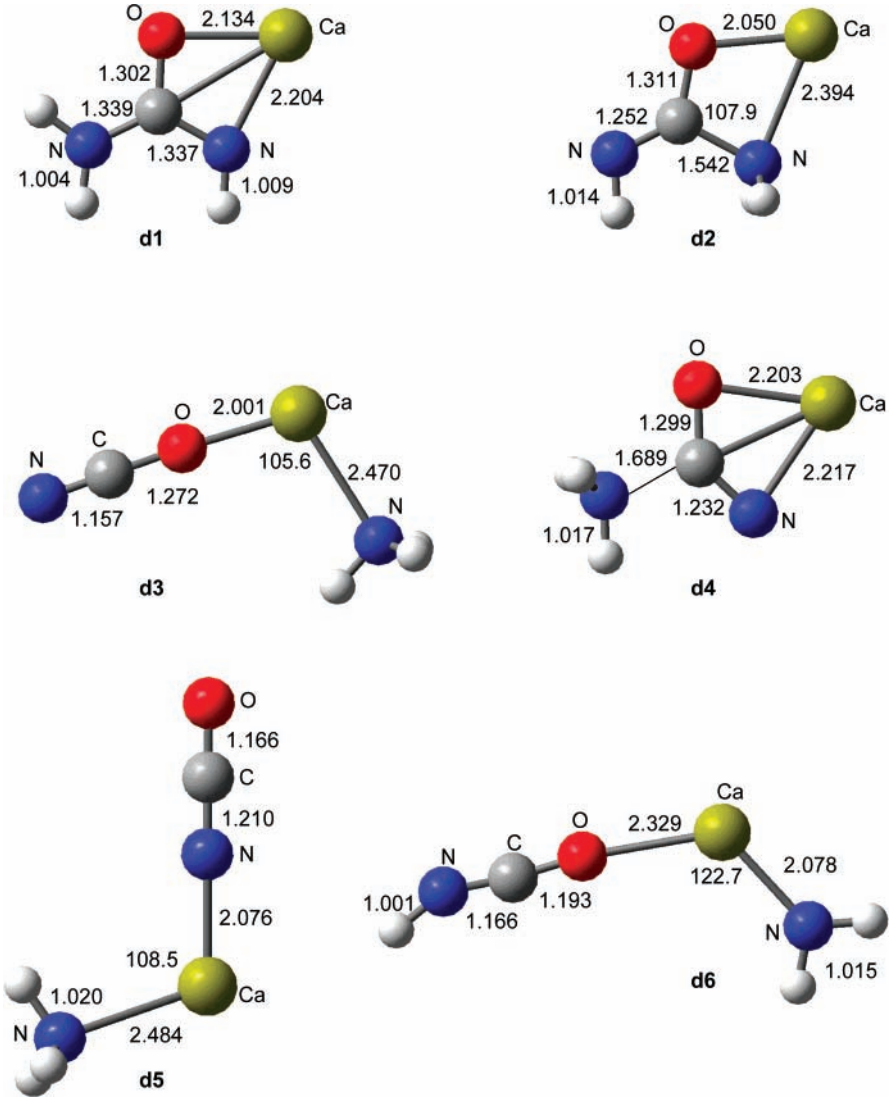

Figure 7. Optimized geometries for isomeric $[Ca(U-H)]^+$ structures. Bond lengths are in angstroms, and bond angles are in degrees.

involving transition structures **TS67** and **TS78**, to finally yield species **8**, which can also dissociate by losing HNCO or NH_3. It should be noted that in the case of the dissociation of **8**, Ca will end up being attached to the NH group of HNCO. This corresponds to a dissociation limit that is 62 kJ mol^{-1} higher in energy than that associated with the unimolecular fragmentation of complex **5** in which Ca ends up being attached to the oxygen atom of HNCO. It is worth noting that these fragmentations in which a doubly charged species is formed can be viewed as a Cooks kinetics experiment.[39,40] Thus, the alternative dissociations of complex **5** to $[Ca-NH_3]^{2+}$ + HNCO or to NH_3 + $[Ca-OCNH]^{2+}$ clearly show that the Ca^{2+} affinity of ammonia is almost identical to that of HNCO if the metal cation attachment takes place at the oxygen atom in the latter case. The fragmentation of complex **8** shows, however, that the Ca^{2+} affinity of HNCO is much smaller when it behaves as a nitrogen base.

Complex **6** is a good precursor for Coulomb explosion reactions, leading to fragmentation into NH_4^+ + $[Ca, N, C, O]^+$. Two possible pathways can be envisaged involving transition structures **TS6a** and **TS6b**. In both of these transition structures, the imaginary frequency corresponds essentially to a proton transfer from the $HNCOCa^{2+}$ moiety toward the NH_3 fragment. The main difference between **TS6a** and **TS6b** is that the former is produced after a Ca−N bond cleavage in **6** and the latter is produced after a Ca−O bond fission. Accordingly, in the former case Ca is attached to the oxygen atom in the $CaOCN^+$ product ion, whereas in the latter case it is attached to the nitrogen atom. Interestingly, the barrier for producing $CaNCO^+$ (via **TS6b**) is slightly higher (by 12 kJ mol^{-1}) than that required to produce $CaOCN^+$ (via **TS6a**), even though the former is strongly favored thermodynamically (by 106 kJ mol^{-1}). Because of the relatively similar barriers, the peak observed at *m*/*z* 82 is likely to correspond to a mixture of the $CaOCN^+$ and $CaNCO^+$ isomers.

In light of these results, one should also expect a partner peak of equal intensity to the *m*/*z* 82 peak at *m*/*z* 18, corresponding to NH_4^+. However, this is not seen. If one considers two isobaric singly charged and doubly charged ions, then the doubly charged ion has twice the axial kinetic energy of the singly charged ion for a given potential difference. As a consequence, product ions generated by a Coulomb explosion of a doubly charged ion should gain much more radial energy than a normal singly charged ion generated from a simple neutral loss. In this connection, Kondow and co-workers[41] noticed during their study of $[Ca(EtOH)_n]^{2+}$ clusters that product ions generated by Coulomb explosion have much larger velocities than the other ions. Furthermore, the NH_4^+ ions, because of their smaller mass, will gain the main part of the radial energy and therefore will have a much higher velocity than *m*/*z* 82. This may result in an unstable trajectory within the instrument that could explain why

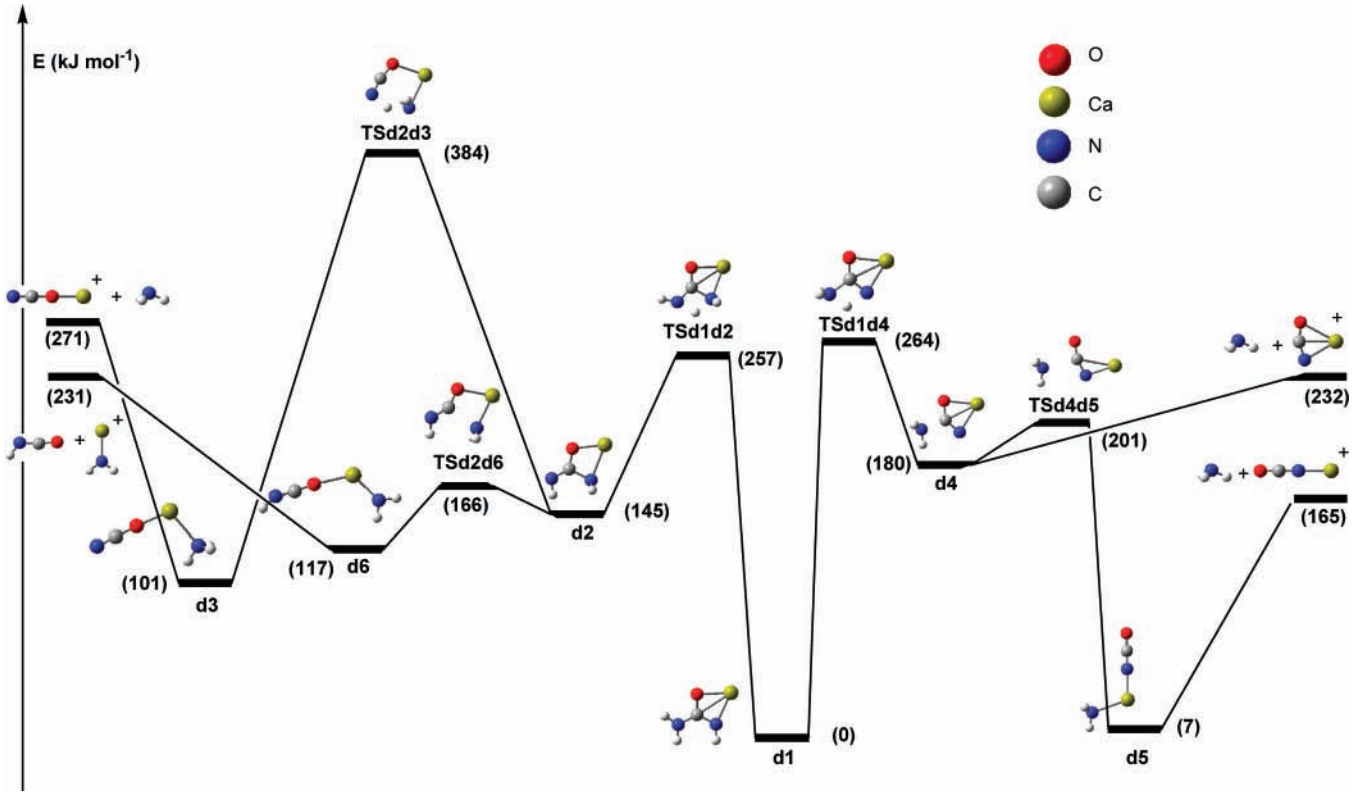

Figure 8. Schematic energy profile associated with unimolecular rearrangements and fragmentations of $[Ca(U-H)]^+$ complexes. Relative energies (kJ mol^{-1}) are in parentheses.

m/*z* 18 is not detected in the MS/MS spectrum. This reasoning seems to be supported by the fact that when NH_4^+ ions are generated from protonated urea (*m*/*z* 61) under rigorously identical conditions to those used in our investigation of $[Ca(\mathbf{U})]^{2+}$ they are easily detected. Furthermore, similar findings have been reported previously in the literature,[42] for example, in the reactions between Ca^{2+} and CH_3CN where a Coulomb explosion yielding $CH_3^+ + CaCN^+$ is observed, but the CH_3^+ cation is not detected.

The *m*/*z* 82 peak could, in principle, arise alternatively from a loss of NH_3 from the $[Ca(U-H)]^+$ molecular cation. However, our theoretical estimates indicate that the deprotonation process for the $[Ca(U)]^{2+}$ complex is endothermic by 107 kJ mol^{-1}. This is indeed consistent with the absence of *m*/*z* 99 peaks in the corresponding MS/MS spectrum.

The presence of two peaks at *m*/*z* 56 and 44 in the MS/MS spectrum suggests the existence of other Coulomb explosions. Two possibilities that would be consistent with the presence of these two peaks are the fragmentation into $CaO^+ + [H_2NCNH_2]^+$ or into $[CaNH_2]^+ + [H_2NCO]^+$. The former can have its origin in the global minimum **1**, whose C═O bond, as mentioned in preceding sections, is weaker than that in free urea. However, this process is unlikely to occur because it involves a barrier (through **TS1a**) more than 210 kJ mol^{-1} above the entrance channel, reflecting the still considerable strength of the C═O bond in a carbonyl group. Alternatively, the fragmentation of structure **2** into $[CaNH_2]^+ + [H_2NCO]^+$ requires a barrier, via transition structure **TS2a**, that lies 186 kJ mol^{-1} below the entrance channel. This is consistent with the significant weakening that accompanies Ca^{2+} attachment of the C−N bond that is cleaved in this process. Hence, our calculations suggest that the *m*/*z* 44 peak corresponds to the $[H_2NCO]^+$ cation whereas the *m*/*z* 56 peak corresponds to the $[CaNH_2]^+$ complex.

Finally, it is worth noting from Figure 6 that because of the high urea−Ca^{2+} binding energy the entire PES (other than **TS1a**) lies below the entrance channel. This is consistent with the loss of urea being observed to only a very minor extent and at high collision energies in the MS/MS spectrum.

Mechanisms for the Unimolecular Reactions of $[Ca(U-H)]^+$ Ions. As mentioned above, the deprotonation of $[Ca(U)]^{2+}$ complexes is not observed. However, the $[Ca(U-H)]^+$ ions are easily produced from $[Ca(U)_n]^{2+}$ ($n = 2$ or 3) complexes by increasing the declustering potential. We thought it to be of interest to investigate if there are significant differences between the unimolecular reactivity of the $[Ca(U)]^{2+}$ dications and that of the corresponding deprotonated monocation.

The geometries of minimum-energy structures **d1**−**d6** are displayed in Figure 7, and those for the other stationary points, together with total energies and ZPVE corrections for all of the stationary points, are given in Tables S3 and S4 of the Supporting Information. The profile for the PES associated with the unimolecular reactivity of $[Ca(U-H)]^+$ is shown in Figure 8.

In the global minimum **d1**, the metal binds simultaneously to the nitrogen of the imino group and to the oxygen of the carbonyl group. From here, two nonequivalent hydrogen shifts may take place. The one that requires a lower barrier corresponds to a 1,3-H shift from the amino to the imino group to yield the local minimum **d2**. A cleavage of its C−NH_2 bond leads to **d6** that can then dissociate into HNCO + $[CaNH_2]^+$, which is experimentally observed. The alternative hydrogen migration in **d2** to yield **d3** requires a high barrier. Thus, the observed loss of NH_3 is not likely to come from a dissociation of **d3** but from another precursor. Indeed, the hydrogen shift from the imino group to the amino group in **d1**, via transition structure **TSd1d4**, leads to local minimum **d4** where the C···NH_3 bond is significantly elongated, thus resulting in the easy

loss of ammonia. A second mechanism that originates in **d4** follows from the migration of the NH_3 fragment toward the Ca via **TSd4d5**. The very stable complex formed, **d5**, can also dissociate by losing NH_3, which is accompanied by $CaNCO^+$ as the product ion. Hence, in agreement with the experimental findings, the unimolecular reactivity of $[Ca(U-H)]^+$ differs from that of $[Ca(U)]^{2+}$ complexes largely through the absence of the Coulomb explosion processes, which of course are possible only for the doubly charged species.

Conclusions

The unimolecular reactivity of $[Ca(U)]^{2+}$ and $[Ca(U-H)]^+$ produced in the gas-phase reactions between Ca^{2+} and urea are rather alike in the sense that both lose ammonia and HNCO in similar relative proportions. The main difference in the observed reactivities is the presence in the dication of Coulomb explosion processes that cannot occur in the singly charged ion. An analysis of the $[Ca(U)]^{2+}$ potential energy surface suggests that the ions produced in these Coulomb explosions are $CaNH_2^+$, H_2NCO^+, $[Ca, N, C, O]^+$, and NH_4^+. In the case of the $[Ca, N, C, O]^+$ product ions, isomers in which the metal is attached either to the nitrogen ($CaNCO^+$) or to the oxygen atom ($CaOCN^+$) are possible, the former lying significantly lower in energy.

For $[Ca(U)]^{2+}$, the unimolecular processes leading to the loss of NH_3 and HNCO involve 1,3-H shifts between the two amino groups. For $[Ca(U-H)]^+$ complexes, the 1,3-H shift from the amino group toward the imino group is associated with the loss of HNCO, whereas the 1,3-H shift from the imino to the amino group leads to the loss of NH_3.

Urea behaves as an oxygen base with respect to Ca^{2+}, the calculated binding energy being 453 kJ mol^{-1}.

Acknowledgment. This work has been partially supported by DGI project no. BQU2003-00894, by the COST Action D26/0014/03, and by the Acción Integrada Hispano-Francesa HF2001-0042. I.C. gratefully acknowledges an FPU grant from the Ministerio de Educación, Cultura y Deporte of Spain. O.M. thanks the Ministerio of Educación, Cultura y Deporte of Spain for a Visiting Fellowship to the University of Sydney. L.R. thanks the Australian Research Council for a Discovery Grant and gratefully acknowledges a generous allocation of computer time on the Compaq Alphaserver of the ANU Supercomputing Facility and the National Facility of the Australian Partnership for Advanced Computing.

Supporting Information Available: Optimized geometries (Cartesian coordinates) of the transition structures and total energies and zero-point vibrational energies of all of the stationary points on the $[Ca(U)]^{2+}$ and $[Ca(U-H)]^+$ potential energy surfaces. This material is available free of charge via the Internet at http://pubs.acs.org.

References and Notes

(1) *Metal Ions in Genetic Information Transfer*; Eichhorn, G. L., Marzilli, L. G., Eds.; Advances in Inorganic Biochemistry; Elsevier/North-Holland: New York, 1981; Vol. 3.

(2) *Metal Ions in Biological Systems: Interrelations among Metal Ions, Enzymes, and Gene Expression*; Sigel, A., Sigel, H., Eds.; Marcel Dekker: New York, 1989; Vol. 25.

(3) *Metal Ions in Biological Systems: Interactions of Metal Ions with Nucleotides, Nucleic Acids, and their Constituents*; Sigel, A., Sigel, H., Eds.; Marcel Dekker: New York, 1996; Vol. 32.

(4) *Metal Ions in Biological Systems: Probing of Nucleic Acids by Metal Ion Complexes of Small Molecules*; Sigel, A., Sigel, H., Eds.; Marcel Dekker: New York, 1996; Vol. 33.

(5) Duguid, J.; Bloomfield, V. A.; Benevides, J.; Thomas, G. J., Jr. *Biophys. J.* **1993**, *65*, 1916−1928.

(6) Jia, X.; Marzilli, L. G. *Biopolymers* **1991**, *31*, 23−44.

(7) Basch, H.; Krauss, M.; Stevens, W. J. *J. Am. Chem. Soc.* **1985**, *107*, 7267−7271.

(8) Noguera, M.; Bertrán, J.; Sodupe, M. *J. Phys. Chem. A* **2004**, *108*, 333−341.

(9) Martin, R. B. *Acc. Chem. Res.* **1985**, *18*, 32−37.

(10) Sigel, H. *Chem. Soc. Rev.* **1993**, *22*, 255−267.

(11) Buchman, Y. V.; Draper, D. E. *J. Mol. Biol.* **1997**, *273*, 1020−1025.

(12) Burda, J. V.; Sponer, J.; Hobza, P. *J. Phys. Chem.* **1996**, *100*, 7250−7255.

(13) Russo, N.; Toscano, M.; Grand, A. *J. Phys. Chem. A* **2003**, *107*, 11533−11538.

(14) Burda, J. V.; Sponer, J.; Leszczynski, J.; Hobza, P. *J. Phys. Chem. B* **1997**, *101*, 9670−9677.

(15) Sponer, J.; Sabat, M.; Burda, J. V.; Leszczynski, J.; Hobza, P. *J. Phys. Chem. B* **1999**, *103*, 2528−2534.

(16) Buckin, V. A.; Kankiya, B. I.; Rentzeperis, D.; Marky, L. A. *J. Am. Chem. Soc.* **1994**, *116*, 9423−9429.

(17) Sponer, J.; Burda, J. V.; Sabat, M.; Leszczynski, J.; Hobza, P. *J. Phys. Chem. A* **1998**, *102*, 5951−5957.

(18) Muñoz, J.; Sponer, J.; Hobza, P.; Orozco, M.; Luque, F. J. *J. Phys. Chem. B* **2001**, *105*, 6051−6060.

(19) Rulísek, L.; Sponer, J. *J. Phys. Chem. B* **2003**, *107*, 1913−1923.

(20) Magnusson, E. *J. Phys. Chem.* **1994**, *98*, 12558−12569.

(21) Petrie, S. *J. Phys. Chem. A* **2002**, *106*, 7034−7041.

(22) Merril, G. N.; Webb, S. P.; Bivin, D. B. *J. Phys. Chem. A* **2003**, *107*, 386-396.

(23) Jayaweera, P.; Blades, A. T.; Ikonomou, M. G.; Kebarle, P. *J. Am. Chem. Soc.* **1990**, *112*, 2452−2454.

(24) Luna, A.; Amekraz, B.; Morizur, J. P.; Tortajada, J.; Mo, O.; Yanez, M. *J. Phys. Chem. A* **1997**, *101*, 5931−5941.

(25) Luna, A.; Amekraz, B.; Tortajada, J.; Morizur, J. P.; Alcami, M.; Mo, O.; Yanez, M. *J. Am. Chem. Soc.* **1998**, *120*, 5411−5426.

(26) Luna, A.; Amekraz, B.; Morizur, J. P.; Tortajada, J.; Mo, O.; Yanez, M. *J. Phys. Chem. A* **2000**, *104*, 3132−3141.

(27) Alcamí, M.; Luna, A.; Mo, O.; Yáñez, M.; Boutreau, L.; Tortajada, J. *J. Phys. Chem. A* **2002**, *106*, 2641−2651.

(28) Corral, I.; Mó, O.; Yáñez, M.; Scott, A. P.; Radom, L. *J. Phys. Chem. A* **2003**, *107*, 10456−10461.

(29) Koch, W.; Holthausen, M. C. *A Chemist's Guide to Density Functional Theory*; Wiley-VCH: Weinheim, Germany, 2000.

(30) Frisch, M. J.; Trucks, G. W.; Schlegel, H. B.; Scuseria, G. E.; Robb, M. A.; Cheeseman, J. R.; Zakrzewski, V. G.; Montgomery, J. A., Jr.; Stratmann, R. E.; Burant, J. C.; Dapprich, S.; Millam, J. M.; Daniels, A. D.; Kudin, K. N.; Strain, M. C.; Farkas, O.; Tomasi, J.; Barone, V.; Cossi, M.; Cammi, R.; Mennucci, B.; Pomelli, C.; Adamo, C.; Clifford, S.; Ochterski, J.; Petersson, G. A.; Ayala, P. Y.; Cui, Q.; Morokuma, K.; Malick, D. K.; Rabuck, A. D.; Raghavachari, K.; Foresman, J. B.; Cioslowski, J.; Ortiz, J. V.; Stefanov, B. B.; Liu, G.; Liashenko, A.; Piskorz, P.; Komaromi, I.; Gomperts, R.; Martin, R. L.; Fox, D. J.; Keith, T.; Al-Laham, M. A.; Peng, C. Y.; Nanayakkara, A.; Gonzalez, C.; Challacombe, M.; Gill, P. M. W.; Johnson, B. G.; Chen, W.; Wong, M. W.; Andres, J. L.; Head-Gordon, M.; Replogle, E. S.; Pople, J. A. *Gaussian 98*, revision A.3; Gaussian, Inc.: Pittsburgh, PA, 1998.

(31) Becke, A. D. *J. Chem. Phys.* **1993**, *98*, 5648−5652.

(32) Lee, C.; Yang, W.; Parr, R. G. *Phys. Rev. B: Condens. Matter* **1988**, *37*, 785−789.

(33) Iron, M. A.; Oren, M.; Martin, J. M. L. *Mol. Phys.* **2003**, *101*, 1345−1361.

(34) Martin, J. M. L.; de Oliveira, G. *J. Chem. Phys.* **1999**, *111*, 1843−1856.

(35) Gonzalez, C.; Schlegel, H. B. *J. Chem. Phys.* **1989**, *90*, 2154−2161.

(36) Bader, R. F. W. *Atoms in Molecules: A Quantum Theory*; Clarendon Press: Oxford, England, 1990.

(37) Schröder, D.; Weiske, T.; Schwarz, H. *Int. J. Mass. Spectrom.* **2002**, *219*, 729−738.

(38) Rodriguez-Santiago, L.; Sodupe, M.; Salpin, J.-Y.; Tortajada, J. *J. Phys. Chem. A* **2003**, *107*, 9685−9874.

(39) McLuckey, S. A.; Cameron, D.; Cooks, R. G. *J. Am. Chem. Soc.* **1981**, *103*, 1313−1317.

(40) Cooks, R. G.; Patrick, J. S.; Kotiaho, T.; McLuckey, S. A. *Mass Spectrom. Rev.* **1994**, *13*, 287−339.

(41) Kohno, J.; Mafune, F.; Kondow, T. *J. Phys. Chem. A* **1999**, *103*, 1518−1522.

(42) Kohler, M.; Leary, J. A. *Int. J. Mass Spectrom. Ion Processes* **1997**, *162*, 17−34.